

Dynamic equilibrium between closed and partially closed states of the bacterial Enzyme I unveiled by solution NMR and X-ray scattering

Vincenzo Venditti^{a,b,1}, Charles D. Schwieters^{c,1}, Alexander Grishaev^{a,2}, and G. Marius Clore^{a,3}

^aLaboratory of Chemical Physics, National Institute of Diabetes and Digestive and Kidney Diseases, National Institutes of Health, Bethesda, MD 20892-0520; ^bDepartment of Chemistry, Iowa State University, Ames, IA 50011; and ^cDivision of Computational Biosciences, Center for Information Technology, National Institutes of Health, Bethesda, MD 20892-5624

Contributed by G. Marius Clore, August 4, 2015 (sent for review July 27, 2015; reviewed by Hashim M. Al-Hashimi)

Enzyme I (EI) is the first component in the bacterial phosphotransferase system, a signal transduction pathway in which phosphoryl transfer through a series of bimolecular protein–protein interactions is coupled to sugar transport across the membrane. EI is a multidomain, 128-kDa homodimer that has been shown to exist in two conformational states related to one another by two large (50–90°) rigid body domain reorientations. The open conformation of apo EI allows phosphoryl transfer from His189 located in the N-terminal domain α/β ($EIN^{\alpha/\beta}$) subdomain to the downstream protein partner bound to the EIN^{α} subdomain. The closed conformation, observed in a trapped phosphoryl transfer intermediate, brings the $EIN^{\alpha/\beta}$ subdomain into close proximity to the C-terminal dimerization domain (EIC), thereby permitting in-line phosphoryl transfer from phosphoenolpyruvate (PEP) bound to EIC to His189. Here, we investigate the solution conformation of a complex of an active site mutant of EI (H189A) with PEP. Simulated annealing refinement driven simultaneously by solution small angle X-ray scattering and NMR residual dipolar coupling data demonstrates unambiguously that the EI(H189A)–PEP complex exists in a dynamic equilibrium between two approximately equally populated conformational states, one corresponding to the closed structure and the other to a partially closed species. The latter likely represents an intermediate in the open-to-closed transition.

multidomain protein dynamics | dipolar couplings | X-ray scattering | conformational states | ligand binding

Enzyme I (EI) is the first component of the bacterial phosphoenolpyruvate (PEP):sugar phosphotransferase signal transduction system (PTS) whereby transfer of sugars across the membrane is coupled to a sequential phosphorylation cascade involving a series of bimolecular protein–protein interactions (1). Autophosphorylation of EI by PEP activates the PTS. Under conditions of nitrogen limitation, competitive inhibition of EI by α -ketoglutarate, an analog of PEP, abolishes sugar uptake by the PTS, thereby providing a regulatory link between central carbon and nitrogen metabolism (2, 3).

EI is a 128-kDa homodimer, with each subunit comprising two domains (4–6) (Fig. 1A). The N-terminal domain (EIN) is itself subdivided into two subdomains: EIN^{α} includes the binding site for the His phosphocarrier protein (HPr), the downstream partner in the phosphorylation cascade, and $EIN^{\alpha/\beta}$ contains the site of phosphorylation at His189 (7–9). The C-terminal dimerization domain (EIC) possesses the PEP binding site (10–13). EIN^{α} and $EIN^{\alpha/\beta}$ are connected to one another by two extended loops (7–9), whereas $EIN^{\alpha/\beta}$ is connected to EIC via a long swivel helix (14, 15) (Fig. 1A). The structures of free EI from *Escherichia coli* and *Staphylococcus aureus* in solution (16, 17) and crystal states (15) display open conformations (Fig. 1A, *Left*), whereas the structure of a trapped phosphoryl transfer intermediate of phosphorylated *E. coli* EI has a closed conformation (14) (Fig. 1A, *Right*). The open-to-closed state transition involves two large rigid body conformational transitions accompanied by an ~ 50 – 70° reorientation of $EIN^{\alpha/\beta}$ relative to EIC and an $\sim 90^\circ$ reorientation of EIN^{α}

relative to $EIN^{\alpha/\beta}$ (16). We refer to the $EIN^{\alpha}/EIN^{\alpha/\beta}$ orientation found in the open and closed structures as the A and B conformations of EIN , respectively. Only the A conformation has been observed in solution and crystal structures of isolated EIN , free (7, 8), complexed to HPr (9), or phosphorylated (18). Modeling suggests that either both domain reorientations occur concurrently or reorientation of $EIN^{\alpha/\beta}$ relative to EIC precedes reorientation of EIN^{α} to avoid a steric clash between EIN^{α} and EIC, resulting in the formation of an intermediate (16).

In the closed structure, the position of $EIN^{\alpha/\beta}$ relative to EIC allows direct in-line phosphoryl transfer from PEP bound to EIC to His189 on $EIN^{\alpha/\beta}$ (14). However, in the orientation of EIN^{α} relative to $EIN^{\alpha/\beta}$ seen in the closed state (i.e., the B conformation of EIN) the C α –C α distance between His189 and His15 of HPr bound to EIN^{α} is too large (~ 30 Å) to permit subsequent phosphoryl transfer from EIN to HPr (16). In the open state of EI, with EIN in the A conformation, however, the reverse holds: the orientation of EIN^{α} to $EIN^{\alpha/\beta}$ places His189 in close proximity to His15 of HPr, thereby permitting in-line phosphoryl transfer to HPr (9). Thus, rapid interconversion between the open and closed states of EI is critical to catalytic function.

Significance

The bacterial phosphotransferase system couples phosphoryl transfer to sugar transport across the cell membrane. The first protein in the pathway, Enzyme I (EI), undergoes two large rigid body domain reorientations between an autophosphorylation-competent closed state and an open state that allows subsequent phosphoryl transfer to its downstream protein partner. Simultaneous use of solution X-ray scattering and NMR dipolar coupling data to guide simulated annealing refinement reveals the existence of a dynamic equilibrium between closed and partially closed conformations in a complex of a mutant of EI with phosphoenolpyruvate. The partially closed conformation represents an intermediate in the open-to-closed transition.

Author contributions: V.V., C.D.S., and G.M.C. designed research; V.V., C.D.S., and A.G. performed research; V.V., C.D.S., and G.M.C. analyzed data; and V.V., C.D.S., and G.M.C. wrote the paper.

Reviewers included: H.M.A., Duke University Medical Center.

The authors declare no conflict of interest.

Data deposition: The atomic coordinates, experimental RDC and SAXS data, and chemical shift assignments have been deposited in the Protein Data Bank, www.pdb.org (PDB ID code 2N5T).

¹V.V. and C.D.S. contributed equally to the work.

²Present address: Institute of Bioscience and Biotechnology Research, University of Maryland, Rockville, MD 20850.

³To whom correspondence should be addressed. Email: mariusc@mail.nih.gov.

This article contains supporting information online at www.pnas.org/lookup/suppl/doi:10.1073/pnas.1515366112/-DCSupplemental.

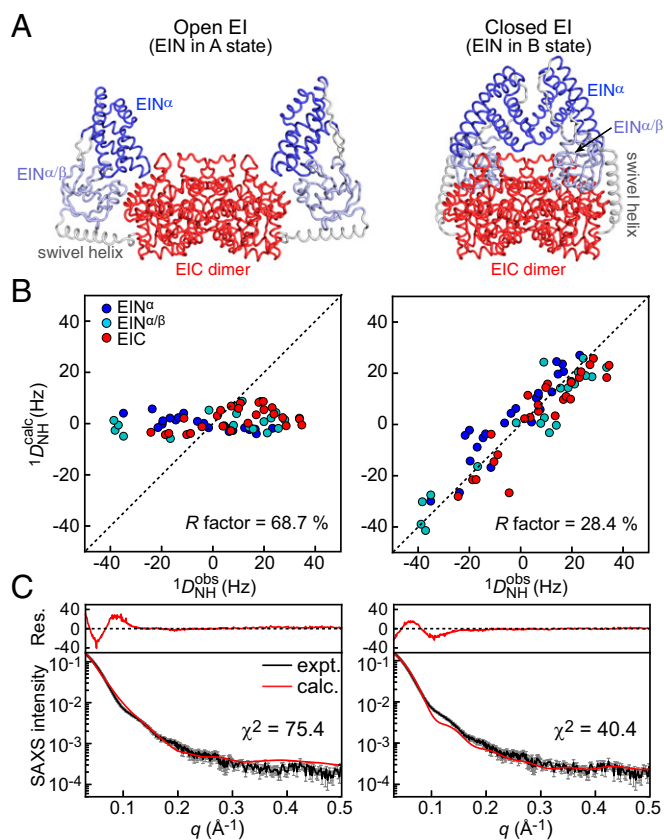


Fig. 1. Agreement of the experimental RDC and SAXS data acquired for the EI^A-PEP complex with the EI^{open} and EI^{closed} structures. (A) NMR structure of EI^{open} [Left; PDB ID code 2KX9 (16)] and X-ray structure of EI^{closed} [Right, trapped phosphoryl transfer intermediate; PDB ID code 2HWG (14)]. EIN α , EIN α/β , and EIC are colored blue, light blue, and red, respectively. (B) Agreement between the experimental ($^1D_{NH}^{obs}$) RDCs for the EI^A-PEP complex and the back-calculated ($^1D_{NH}^{calc}$) RDCs for the EI^{open} (Left) and EI^{closed} (Right) structures obtained by predicting the alignment tensor from molecular shape. Data points are colored blue, light blue, and red for EIN α , EIN α/β , and EIC, respectively. (C) Agreement between experimental SAXS curve (black) for the EI^A-PEP complex and the back-calculated curves (red) for the EI^{open} (Left) and EI^{closed} (Right) structures. The residuals, given by $(I_i^{calc} - I_i^{obs})/I_i^{err}$, are plotted above the SAXS curves. Error bars: 1 SD.

We recently showed that the open/closed interconversion of PEP-bound EI is modulated by the volume of the active site side chain at position 189, with smaller side chains favoring the closed conformation (19). In the wild-type EI (EI^{WT})-PEP complex, the latter is undetectable in solution by small angle X-ray scattering (SAXS) (19) despite the fact that the closed conformation could be selectively crystallized from a solution of EI, PEP, and Mg²⁺ in which the autophosphorylation reaction was quenched by the inhibitor oxalate (14). These observations can be attributed to steric and electrostatic repulsion between phosphorylated His189 and bound PEP (19), and they emphasize that the crystallized phosphoryl transfer intermediate represents a sparsely populated state in solution. No such clash exists for the EI(H189A) mutant (EI^A), and initial SAXS analysis suggests that the EI^A-PEP complex is skewed toward the closed conformation (~60%); however, a mixture of closed and open states does not accurately reproduce the observed SAXS curve (19) or fully account for the residual dipolar coupling (RDC) data measured by NMR (this work).

Here, on the basis of the known structures of the individual domains of EI, we investigate the solution structure of the EI^A-PEP complex by rigid body-simulated annealing refinement driven by experimental RDC and SAXS data. This analysis indicates that the

EI^A-PEP complex exists as a rapidly interconverting ensemble of two approximately equally populated conformations comprising closed and partially closed states, and it suggests a functional role for the partially closed state in PEP binding and subsequent pyruvate release following autophosphorylation.

Results and Discussion

RDC Analysis of the Individual Structural Domains. RDCs measure the orientation of bond vectors relative to an external alignment tensor, and therefore provide a very sensitive indicator of both structural quality (20) and relative domain orientations (21). Backbone amide ($^1D_{NH}$) RDCs for uniformly ¹⁵N/²H-labeled EI^A-PEP complex, aligned in a neutral bicelle medium (22), were measured for well-resolved ¹H_N/¹⁵N cross-peaks in the ¹H-¹⁵N transverse relaxation optimized spectroscopy (TROSY) correlation spectrum using the ARTSY (amide RDCs by TROSY) technique (23) (the distribution of measured RDCs is shown in Fig. S1). As in the case of EI^{WT} (16), the observed RDCs for the EIN α and EIN α/β subdomains of the EI^A-PEP complex, treated separately, agree better with the corresponding coordinates from the solution NMR structure of the EIN-HPr complex [Protein Data Bank (PDB) ID code 3EZA (9)] (Table 1) than with the corresponding coordinates from the X-ray structures of either isolated EIN (7) or the full-length EI phosphoryl transfer intermediate [PDB ID code 2HWG (14)]. This improved agreement is simply a reflection of the fact that the structure of the EIN-HPr complex was determined using RDCs, albeit in a charged alignment medium of phage fd (9) (hence, the excellent agreement of

Table 1. SVD analysis of backbone amide ($^1D_{NH}$) RDCs for the EI^A-PEP complex

Domain	No. of RDCs	D_a^{NH} (Hz)	η	R-factor,* %
EIN α	23	-19.3	0.34	21.8
EIN α/β	20	-19.7	0.47	17.7
EIN ^A -state	43	-16.5	0.37	50.9
EIN ^B -state'	43	-19.5	0.37	22.2 [†]
EIN ^B -state''	43	-19.6	0.37	22.0 [†]
EIC ^{monomer}	25	-21.8	0.27	24.6
EIC ^{dimer}	25	-22.3	0.28	25.0
EI ^{open}	68	-5.8	0.46	53.5
EI ^{open} †	68	4.3	0.36	68.7
EI ^{closed}	68	-21.2	0.27	25.8
EI ^{closed} ‡	68	-20.8	0.47	28.4

SVD analysis was carried out using the calcTensor helper of Xplor-NIH (29). The base coordinates for the two subdomains of EIN are taken from the solution structure of the isolated EIN-HPr complex [PDB ID code 3EZA (9)]. The structure of isolated EIN (7-9), as well as the structure of EIN in the context of free intact EI (15, 16), is in the A conformation. The coordinates of the B conformation of EIN observed in the crystal structure of the phosphoryl transfer intermediate (14) were obtained by best-fitting the backbone atoms of the EIN α and EIN α/β subdomains from the solution structure [PDB ID code 3EZA (9)] onto the crystal structure of phosphorylated EI [PDB ID code 2HWG (14)]. The coordinates of EIC and the swivel helix were taken from the crystal structure of phosphorylated EI (PDB ID code 2HWG), with protons added using Xplor-NIH (29).

*RDC R-factor is given by $[\langle (D_{obs} - D_{calc})^2 \rangle / (2 \langle D_{obs}^2 \rangle)]^{1/2}$, where D_{obs} and D_{calc} are the observed and calculated RDCs, respectively (30). R-factors for fits showing good agreement between the coordinates and experimental RDCs are shown in bold. D_a^{NH} (in units of Hz) and η are the magnitude of the axial component of the alignment tensor and the rhombicity, respectively.

[†]Orientation of the EIN α subdomain relative to the EIN α/β subdomain is slightly different (by a rotation of 5.4°) in the two subunits of the X-ray structure of phosphorylated EI (14); SVD analysis was therefore performed separately for the two subunits (denoted as ' and '').

[‡]These results were calculated using the SARDC facility in Xplor-NIH (29), which computes the alignment tensor from molecular shape rather than using it as a set of fit parameters as in the case of SVD.

Table 2. RDC and SAXS analysis of the EI^A-PEP complex

Structure	RDC <i>R</i> -factor, %			SAXS*	
	EIN ^α	EIN ^{α/β}	EIC	EI	χ ²
Back-calculation of RDC and SAXS data from the EI ^{open} and EI ^{closed} structures [†]					
EI ^{open}	79.0	67.2	62.6	68.7	75.4
EI ^{closed}	35.1	23.0	29.8	28.4	43.5
EI ^{mix†}	34.2	24.7	34.6	30.2	36.8
Structure refinement of EI ^A -PEP complex against RDC and SAXS data [‡]					
<i>N</i> _e = 1 ^(SAXS)	72.0 ± 0.1	70.2 ± 0.5	62.0 ± 0.6	68.1 ± 0.4	2.1 ± 0.1
<i>N</i> _e = 1 ^(RDC)	22.3 ± 0.1	19.1 ± 0.1	25.3 ± 0.1	22.0 ± 0.1	30.3 ± 9.4
<i>N</i> _e = 1 ^(RDC/SAXS)	25.0 ± 0.3	19.9 ± 0.2	25.2 ± 0.0	23.0 ± 0.1	6.7 ± 0.2
<i>N</i> _e = 2 ^{(RDC/SAXS)*} ¶	22.3 ± 0.1	20.1 ± 0.1	25.4 ± 0.1	22.4 ± 0.1	1.0 ± 0.0
<i>N</i> _e = 3 ^{(RDC/SAXS)*} ¶	22.0 ± 0.0	19.4 ± 0.1	25.5 ± 0.1	22.1 ± 0.1	1.0 ± 0.0

Numbers of RDCs are 23 for EIN^α, 20 for EIN^{α/β}, 25 for EIC, and 68 for the whole EI. Target values of the RDC *R*-factors for EIN^α, EIN^{α/β}, and dimeric EIC, obtained by SVD against the corresponding coordinates, are 21.8%, 17.7%, and 25.0%, respectively (Table 1). The target value for the complete EI dimer, given by the weighted average of the RDC *R*-factors for the individual domains, is 21.8%. The target value of χ² for the SAXS data is 1.0.

*SAXS curves were back-calculated from the coordinates of the EI structures using the calcSAXS-bufsub helper function (19) of Xplor-NIH (29).

[†]RDCs arising from steric alignment were back-calculated from the molecular shapes generated from the coordinates of the EI structures using the calcSARDC helper function of Xplor-NIH (29).

[‡]EI^{Mix} is a two-member ensemble of EI^{open} and EI^{closed} with optimized populations of 5% and 95%, respectively.

[§]Average values and corresponding SDs over the 10 lowest target function structures are reported.

[¶]For the *N*_e = 2 ensemble, one member of the ensemble is fixed to the structure of EI^{closed} (14); in the other ensemble member, EIN^α, EIN^{α/β}, and dimeric EIC are allowed to move relative to one another as rigid bodies, by giving residues within the linker regions Cartesian degrees of freedom (main text). Optimized populations for the closed and partially closed members of the ensemble are 51.7 ± 1.1% and 48.3 ± 1.1%, respectively. For the *N*_e = 3 ensemble, a third member, fixed to the coordinates of EI^{open} (16), is added; the optimized populations are 54.5 ± 1.1% (partially closed), 43.1 ± 1.2% (closed), and 2.4 ± 0.1% (open). Structures of EI^{partially closed} in the *N*_e = 2 and *N*_e = 3 ensembles are the same within experimental error: when fit to the EIC dimer, the C^α rms difference between the EIN domains of the *N*_e = 2 and *N*_e = 3 partially closed structures is only 1.3 ± 0.2 Å.

the RDCs measured in bicelles provides independent cross-validation of the structure), whereas the two crystal structures (7, 14) were solved at a relatively modest resolution (2.5–2.7 Å). Consequently, the NMR coordinates (PDB ID code 3EZA) for EIN^α and EIN^{α/β} were used for all subsequent analyses and to generate the EIN portion of the closed and open structures, whereas the X-ray coordinates (PDB ID code 2HWG) were used for EIC and the swivel helix (footnotes for Table 1 and *SI Materials and Methods*).

Singular value decomposition (SVD) fits of the ¹*D*_{NH} RDCs obtained for the EI^A-PEP complex to the B-conformation of EIN [i.e., the conformation found in the closed X-ray structure (14)] yields RDC *R*-factors that are only slightly worse than the weighted average of the RDC *R*-factors for EIN^α and EIN^{α/β} individually (~22% vs. ~20%), with comparable values for the magnitude of the axial component (*D*_{a^{NH}}) and rhombicity (η) of the fitted alignment tensors (Table 1). By way of contrast, the A conformation of EIN found in apo EI [open state (16, 17)] and isolated EIN (7–9, 18) results in very poor agreement with the measured RDCs, with an RDC *R*-factor of ~51% (Table 1). Thus, EIN in the EI^A-PEP complex must adopt a conformation or ensemble of conformations that is close to the conformation or ensemble of conformations of the B form found in the closed X-ray structure.

Although no solution structure has been determined for EIC, there is excellent agreement between the measured RDCs for the EI^A-PEP complex and the RDCs back-calculated from the crystal structure of phosphorylated EI (14) with comparable *R*-factors (~25%; Table 1) for both an individual subunit and the dimer. These results are fully consistent with previous RDC data obtained for isolated EIC (13), and indicate that the relative orientation of the two EIC domains in the dimeric EI^A-PEP complex is the same as the relative orientation in the crystal structure of phosphorylated EI (14).

RDC and SAXS Analysis of the Full-Length EI^A-PEP Complex. SVD fits of the ¹*D*_{NH} RDCs measured for the EI^A-PEP complex yield *R*-factors of ~54% and ~26% for the open and closed structures of full-length dimeric EI, respectively (Table 1). The latter RDC *R*-factor, however, is significantly larger than the weighted *R*-factor (~22%) obtained when fitting the domains individually. Because the RDCs were measured in a medium (neutral bicelles) where alignment is induced through transient steric interactions, the alignment tensor can be calculated from molecular shape and the RDCs can be back-calculated directly from the molecular coordinates (24–26). Although this approach results in a slightly poorer fit for the closed structure (*R*-factor ~28%; Fig. 1*B*, *Right*), the values of *D*_{a^{NH}} and η are close to the values obtained from SVD analysis (Table 1). In contrast, the value of *D*_{a^{NH}} predicted from the open structure is fivefold smaller and of opposite sign (Table 1), and there is no agreement between observed and back-calculated RDCs (*R*-factor ~69%; Fig. 1*B*, *Left*). One can therefore conclude that the EI^A-PEP complex adopts a conformation(s) that is similar to the conformation of the closed structure.

SAXS, however, reveals a more complex picture, because neither the open (χ² ~75) nor closed (χ² ~44) structures of EI are consistent with the experimental SAXS curve for the EI^A-PEP complex (Fig. 1*C* and Table 2). Moreover, a linear combination of open and closed structures (with optimized populations of 5% and 95%, respectively) results in only minimal improvement, in agreement with the experimental SAXS data (χ² ~37; Table 2) and a slight worsening of the agreement with the RDC data (*R*-factor ~30%), indicating that a simple two-state equilibrium between open and closed structures does not represent the state of the EI^A-PEP complex in solution.

Structure Refinement of the EI^A-PEP Complex. To determine the 3D structure of the EI^A-PEP complex in solution, we therefore made use of RDC- and SAXS-driven rigid body simulated

annealing in which EIN^α , $EIN^{\alpha/\beta}$, and the EIC dimer were treated as separate rigid bodies, whereas the linker regions connecting $EIN^{\alpha/\beta}$ to EIN^α (residues 22–24 and 143–146) and EIC (residues 255–261) were given Cartesian degrees of freedom (full details of the calculational strategy are provided in *SI Materials and Methods*). Allowing backbone deformations of the rigid bodies is not justified because agreement between observed and calculated RDCs at the individual subdomain/domain level (as discussed above) is within the error of the measured RDCs and structure coordinates.

Similar calculations were used to investigate the solution structure of EI^{WT} (16) and the $EI(H189Q)$ mutant (17). However, in the current work, the RDC alignment tensor was calculated directly from the coordinates and molecular shape at every step of molecular dynamics and minimization, as was described in our recent work on the HIV-1 capsid protein (26). This aspect of the calculations is critical because it enables one to carry out ensemble calculations where a single structure is insufficient to account for the experimental data. Further, this approach makes full use of the

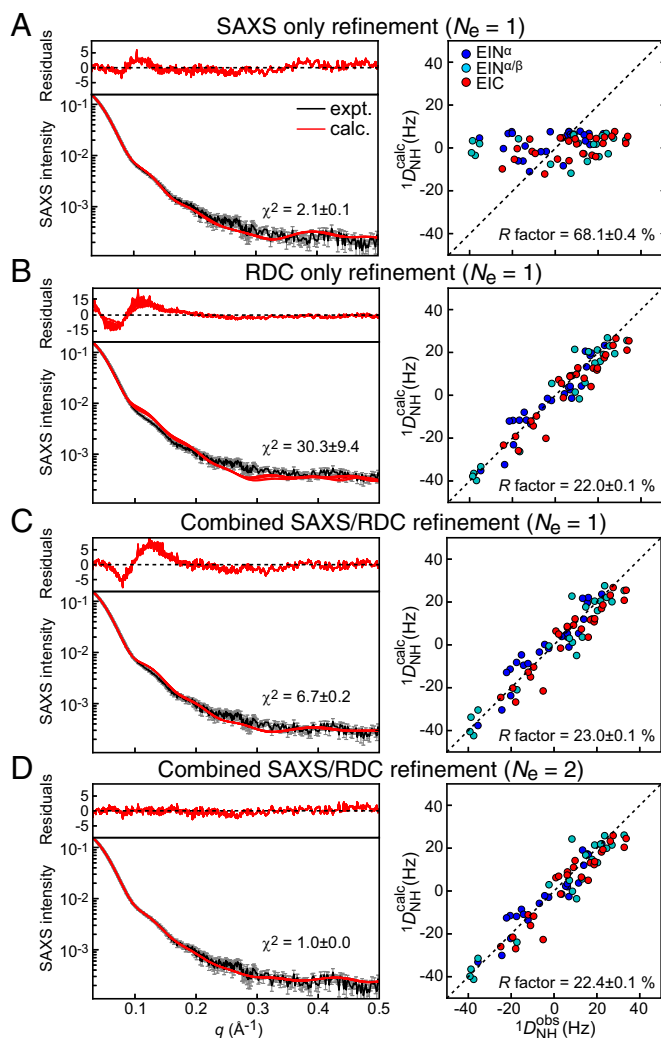


Fig. 2. Structure refinement of the EI^A -EP complex. Comparison of experimental vs. calculated SAXS curves (*Left*) and RDC data (*Right*) for SAXS-only refinement with an ensemble size $N_e = 1$ (A), RDC-only refinement with $N_e = 1$ (B), combined SAXS and RDC refinement with $N_e = 1$ (C), and combined SAXS and RDC refinement with $N_e = 2$ (D). The experimental and calculated (for the 10 lowest target function structures) SAXS curves are shown in black and red, respectively. Error bars: 1 SD. The RDCs for EIN^α , $EIN^{\alpha/\beta}$, and EIC are color-coded blue, light blue, and red, respectively.

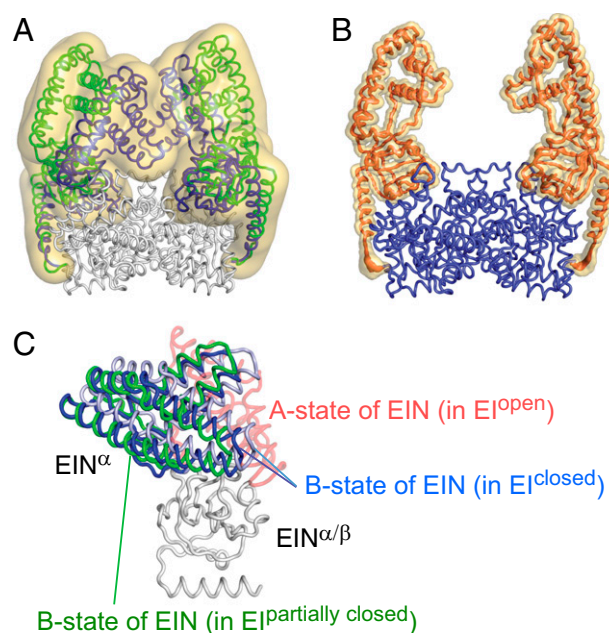


Fig. 3. Structural ensemble of the EI^A -PEP complex obtained from combined refinement against SAXS and RDC data for $N_e = 2$. (A) Overall distribution of EIN relative to EIC displayed as a reweighted atomic probability density map plotted at 2% (transparent yellow surface) of maximum. EIC is shown as a white ribbon. Conformations adopted by EIN in the EI^{closed} and $EI^{partially\ closed}$ states are shown as blue and green ribbons, respectively. (B) Backbone atomic probability density map (plotted at 50% and 2% of maximum in transparent red and yellow, respectively) for $EI^{partially\ closed}$ generated from the $N_e = 2$ calculations. (C) Orientation of EIN^α relative to $EIN^{\alpha/\beta}$ (white ribbon). EIN^α in EI^{open} , EI^{closed} , and $EI^{partially\ closed}$ is displayed in red (transparent), dark blue/light blue (for the two subunits of the X-ray structure of EI^{closed}), and green, respectively. The C^α rms difference between EIN^α of $EI^{partially\ closed}$ (green) and EI^{closed} (dark blue) is smaller than the C^α rms difference between the dark-blue and light-blue EIN^α subdomains of EI^{closed} : 3.2 Å vs. 5.6 Å (Table S1).

information content present in the RDCs because both molecular shape and bond vector orientations are taken into account. In addition, considerable speedup in the computation of SAXS curves was achieved by decomposition into a small number of rigid bodies, thereby rendering the calculation independent of the number of atoms. Specifically, for atoms within a rigid body, the relative atom positions do not change; thus, after an initial calculation, the corresponding contribution to the scattering amplitude can be computed without referring to atomic positions (details are provided in *SI Materials and Methods*).

Three calculations were carried out with an ensemble size of $N_e = 1$ (i.e., a single dimeric structure) and symmetry imposed (Figs. 2 and 3 and Table 2; details of symmetry restraints are provided in *SI Materials and Methods*). Refinement against only the SAXS data results in a structure that satisfies the SAXS curve reasonably well ($\chi^2 = 2.1$) but fails to account for the RDC data (R -factor $\sim 68\%$) (Fig. 2A); refinement against only the RDC data results in a structure that satisfies the RDC data (R -factor = 22%) but fails to reproduce the SAXS data ($\chi^2 = 30$) (Fig. 2B); and combined SAXS and RDC refinement results in a reasonable RDC R -factor (23%) but still fails to satisfy the SAXS data within experimental error ($\chi^2 = 6.7$) (Fig. 2C). One can therefore conclude that the EI^A -PEP complex in solution must adopt several conformations because a single-structure representation does not simultaneously reproduce the experimental RDC and SAXS data. Interconversion between these multiple conformations must be fast on the chemical shift time scale (i.e., submilliseconds) because only a single set of cross-peaks is observed in the 1H - ^{15}N TROSY correlation

autophosphorylation by PEP and the predominant open state in solution needed to effect subsequent phosphoryl transfer to the downstream partner protein HPr.

From a purely experimental perspective, the existence of a dynamic equilibrium between two distinct states of the EI^A-PEP complex could not be ascertained from SAXS or RDC measurements alone because these data, when treated independent of one another, can each be accounted for reasonably well by a single-structure representation. It is only when the SAXS and RDC data are treated together that the existence of a conformational ensemble consisting of two distinct states is revealed, thereby unambiguously demonstrating the dynamic character of the EI^A-PEP complex.

Materials and Methods

Protein Expression and Purification. The H189A mutant of *E. coli* EI (EI^A) was created using the QuikChange Site-Directed Mutagenesis Kit (Stratagene) and expressed and purified as described for EI^{WT} (16).

SAXS. SAXS data were acquired at the Advanced Photon Source (Argonne National Laboratory) on samples of EI^A (5 mg/ml corresponding to ~40 μM dimer) in 20 mM Tris buffer (pH 7.4), 100 mM NaCl, 10 mM DTT, 4 mM MgCl₂, 1 mM EDTA, and one tablet of protease inhibitor mixture (SigmaFAST S8830; Sigma-Aldrich).

1. Clore GM, Venditti V (2013) Structure, dynamics and biophysics of the cytoplasmic protein-protein complexes of the bacterial phosphoenolpyruvate: Sugar phosphotransferase system. *Trends Biochem Sci* 38(10):515–530.
2. Doucette CD, Schwab DJ, Wingreen NS, Rabinowitz JD (2011) α-Ketoglutarate coordinates carbon and nitrogen utilization via enzyme I inhibition. *Nat Chem Biol* 7(12):894–901.
3. Venditti V, Ghirlando R, Clore GM (2013) Structural basis for enzyme I inhibition by α-ketoglutarate. *ACS Chem Biol* 8(6):1232–1240.
4. Chauvin F, Brand L, Roseman S (1994) Sugar transport by the bacterial phosphotransferase system. Characterization of the Escherichia coli enzyme I monomer/dimer transition kinetics by fluorescence anisotropy. *J Biol Chem* 269(32):20270–20274.
5. Chauvin F, Brand L, Roseman S (1996) Enzyme I: The first protein and potential regulator of the bacterial phosphoenolpyruvate: Glycose phosphotransferase system. *Res Microbiol* 147(6–7):471–479.
6. Chauvin F, Fomenkov A, Johnson CR, Roseman S (1996) The N-terminal domain of Escherichia coli enzyme I of the phosphoenolpyruvate/glycose phosphotransferase system: molecular cloning and characterization. *Proc Natl Acad Sci USA* 93(14):7028–7031.
7. Liao DI, et al. (1996) The first step in sugar transport: crystal structure of the amino terminal domain of enzyme I of the *E. coli* PEP: sugar phosphotransferase system and a model of the phosphotransfer complex with HPr. *Structure* 4(7):861–872.
8. Garrett DS, et al. (1997) Solution structure of the 30 kDa N-terminal domain of enzyme I of the Escherichia coli phosphoenolpyruvate:sugar phosphotransferase system by multidimensional NMR. *Biochemistry* 36(9):2517–2530.
9. Garrett DS, Seok YJ, Peterkofsky A, Gronenborn AM, Clore GM (1999) Solution structure of the 40,000 Mr phosphoryl transfer complex between the N-terminal domain of enzyme I and HPr. *Nat Struct Biol* 6(2):166–173.
10. Patel HV, et al. (2006) Properties of the C-terminal domain of enzyme I of the Escherichia coli phosphotransferase system. *J Biol Chem* 281(26):17579–17587.
11. Seok YJ, Zhu PP, Koo BM, Peterkofsky A (1998) Autophosphorylation of enzyme I of the Escherichia coli phosphoenolpyruvate:sugar phosphotransferase system requires dimerization. *Biochem Biophys Res Commun* 250(2):381–384.
12. Oberholzer AE, et al. (2005) Crystal structure of the phosphoenolpyruvate-binding enzyme I-domain from the Thermoanaerobacter tengcongensis PEP: sugar phosphotransferase system (PTS). *J Mol Biol* 346(2):521–532.
13. Venditti V, Clore GM (2012) Conformational selection and substrate binding regulate the monomer/dimer equilibrium of the C-terminal domain of Escherichia coli enzyme I. *J Biol Chem* 287(32):26989–26998.
14. Teplyakov A, et al. (2006) Structure of phosphorylated enzyme I, the phosphoenolpyruvate:sugar phosphotransferase system sugar translocation signal protein. *Proc Natl Acad Sci USA* 103(44):16218–16223.
15. Oberholzer AE, Schneider P, Siebold C, Baumann U, Erni B (2009) Crystal structure of enzyme I of the phosphoenolpyruvate sugar phosphotransferase system in the dephosphorylated state. *J Biol Chem* 284(48):33169–33176.
16. Schwieters CD, et al. (2010) Solution structure of the 128 kDa enzyme I dimer from Escherichia coli and its 146 kDa complex with HPr using residual dipolar couplings and small- and wide-angle X-ray scattering. *J Am Chem Soc* 132(37):13026–13045.
17. Takayama Y, Schwieters CD, Grishaev A, Ghirlando R, Clore GM (2011) Combined use of residual dipolar couplings and solution X-ray scattering to rapidly probe rigid-body conformational transitions in a non-phosphorylatable active-site mutant of the 128 kDa enzyme I dimer. *J Am Chem Soc* 133(3):424–427.

PEP was added to a final concentration of 20 mM immediately before data acquisition (details are provided in *SI Materials and Methods*).

NMR Spectroscopy. NMR samples contained 0.4 mM subunits of EI^A, 50 mM PEP, 20 mM Tris buffer (pH 7.4), 100 mM NaCl, 4 mM MgCl₂, 1 mM EDTA, 2 mM DTT, and 90% H₂O/10% D₂O (vol/vol). Samples were aligned in dimyristoylphosphatidylcholine/06:0 diether phosphatidylcholine bicelles (*q* = 3; Avanti Polar Lipids) doped with 0.1% 1,2-dimyristoyl-*sn*-glycero-3-phosphoethanolamine-*N*-poly(ethylene glycol)2000 (Avanti Polar Lipids) to improve bicelle stability (22). All NMR spectra were recorded at 37 °C at a spectrometer frequency of 800 MHz (details are provided in *SI Materials and Methods*).

Structure Calculations. SAXS- and RDC-driven conjoined rigid body/torsion angle/Cartesian simulated annealing was carried out in Xplor-NIH (16, 28, 29) (details are provided in *SI Materials and Methods*). Coordinates, experimental restraints, and chemical shift assignments have been deposited in the PDB (PDB ID code 2N5T).

ACKNOWLEDGMENTS. We thank Drs. Lixin Fan (National Cancer Institute) and Xiaobing Zuo (Argonne National Laboratory) for their support at the SAXS beamline. This work was supported by the Intramural Programs of the National Institute for Diabetes and Digestive and Kidney Diseases (G.M.C.) and the Center for Information Technology (C.D.S.) at the National Institutes of Health, and by the AIDS Targeted Antiviral Program of the Office of the Director of the National Institutes of Health (G.M.C.).

18. Suh JY, Cai M, Clore GM (2008) Impact of phosphorylation on structure and thermodynamics of the interaction between the N-terminal domain of enzyme I and the histidine phosphocarrier protein of the bacterial phosphotransferase system. *J Biol Chem* 283(27):18980–18989.
19. Venditti V, Tugarinov V, Schwieters CD, Grishaev A, Clore GM (2015) Large inter-domain rearrangement triggered by suppression of micro- to millisecond dynamics in bacterial Enzyme I. *Nat Commun* 6:5960.
20. Bax A, Grishaev A (2005) Weak alignment NMR: A hawk-eyed view of biomolecular structure. *Curr Opin Struct Biol* 15(5):563–570.
21. Clore GM (2000) Accurate and rapid docking of protein-protein complexes on the basis of intermolecular nuclear overhauser enhancement data and dipolar couplings by rigid body minimization. *Proc Natl Acad Sci USA* 97(16):9021–9025.
22. King V, Parker M, Howard KP (2000) Pegylation of magnetically oriented lipid bilayers. *J Magn Reson* 142(1):177–182.
23. Fitzkee NC, Bax A (2010) Facile measurement of ¹H-¹⁵N residual dipolar couplings in larger perdeuterated proteins. *J Biomol NMR* 48(2):65–70.
24. Zweckstetter M, Bax A (2000) Prediction of sterically induced alignment in a dilute liquid crystalline phase: Aid to protein structure determination by NMR. *J Am Chem Soc* 122(15):3791–3792.
25. Huang JR, Grzesiek S (2010) Ensemble calculations of unstructured proteins constrained by RDC and PRE data: A case study of urea-denatured ubiquitin. *J Am Chem Soc* 132(2):694–705.
26. Deshmukh L, et al. (2013) Structure and dynamics of full-length HIV-1 capsid protein in solution. *J Am Chem Soc* 135(43):16133–16147.
27. Braddock DT, Cai M, Baber JL, Huang Y, Clore GM (2001) Rapid identification of medium- to large-scale interdomain motion in modular proteins using dipolar couplings. *J Am Chem Soc* 123(35):8634–8635.
28. Schwieters CD, Clore GM (2014) Using small angle solution scattering data in Xplor-NIH structure calculations. *Prog Nucl Magn Reson Spectrosc* 80(1):1–11.
29. Schwieters CD, Kuszewski J, Clore GM (2006) Using Xplor-NIH for NMR molecular structure determination. *Prog Nucl Magn Reson Spectrosc* 48(1):47–62.
30. Clore GM, Garrett DS (1999) *R*-factor, free *R* and complete cross-validation for dipolar coupling refinement of NMR structures. *J Am Chem Soc* 121(39):9008–9012.
31. Delaglio F, et al. (1995) NMRPipe: A multidimensional spectral processing system based on UNIX pipes. *J Biomol NMR* 6(3):277–293.
32. Schwieters CD, Clore GM (2001) Internal coordinates for molecular dynamics and minimization in structure determination and refinement. *J Magn Reson* 152(2):288–302.
33. Bermejo GA, Clore GM, Schwieters CD (2012) Smooth statistical torsion angle potential derived from a large conformational database via adaptive kernel density estimation improves the quality of NMR protein structures. *Protein Sci* 21(12):1824–1836.
34. Ryabov Y, Suh JY, Grishaev A, Clore GM, Schwieters CD (2009) Using the experimentally determined components of the overall rotational diffusion tensor to restrain molecular shape and size in NMR structure determination of globular proteins and protein-protein complexes. *J Am Chem Soc* 131(27):9522–9531.
35. Renka RJ (1984) Interpolation of data on the surface of a sphere. *ACM Trans Math Softw* 10(4):417–436.
36. Grishaev A, Guo L, Irving T, Bax A (2010) Improved fitting of solution X-ray scattering data to macromolecular structures and structural ensembles by explicit water modeling. *J Am Chem Soc* 132(44):15484–15486.